J. Fluid Mech. (1996), *vol.* 316, *pp.* 115–137

Topological interpretation of the surface flow visualization of conical viscous/inviscid interactions

By B. W. VAN OUDHEUSDEN, C. NEBBELING AND W. J. BANNINK

Delft University of Technology, Dept. Aerospace Engineering, Lab. for High Speed Aerodynamics, PO Box 5058, 2600 GB Delft, The Netherlands

(Received 24 April 1995 and in revised form 20 December 1995)

The asymptotic flow structure is considered for a viscous–inviscid conical interaction, in particular that between a swept shock wave and a boundary layer. A flow model is devised based on the three-layer interaction concept. Assuming conicity of the inviscid flow regions, a viscous layer structure is established that is compatible with the inviscid outer flow, and which produces a geometrically conical surface flow pattern. This result is obtained from a dimensional analysis, which reveals similarity of the viscous layer in cross-flow planes at different radial distances from the conical origin. The results of this analysis provide a tool for the quantitative interpretation of surface flow visualizations in terms of the related topological structure of the flow in the cross-flow plane. This method is illustrated by application to the surface flow visualization of a Mach 3 shock-wave/boundary-layer interaction.

1. Introduction

1.1. *Conical viscous/inviscid interactions*

For geometrically conical configurations, like delta wings, cones, or wedge–plate junctions, the supersonic inviscid flow field can (under appropriate conditions) display a conical symmetry, where flow variables are constant along straight rays emanating from the body vertex (Bulakh 1970). The conical flow similarity is essentially restricted to inviscid flow, and is absent in viscous flow due to the length dependence of the shear stress terms. Notwithstanding this, the interaction between a nearly inviscid outer flow and a viscosity-dominated surface flow has often been observed to result in (near) conicity of the surface flow pattern, e.g. for the surface pressure and skin friction directions.

An important class of conical flows is that resulting from the interaction between a swept shock wave and a boundary layer (see figure 1). In practice this occurs, for example, for shock waves generated by the leading edge of aircraft wings, at the inlet of a supersonic diffusor or between the blades of a turbine cascade. The (asymptotic) conicity of this type of interaction has been revealed in an abundance of experimental and numerical studies, see recent reviews by Settles (1993) and Knight (1993). Relatively little attention has been given to the theoretical description of the underlying asymptotic structure, apart from the study by Inger (1987) where the far field of the conical interaction was, however, incorrectly argued to possess a quasi-two-dimensional structure in the cross-flow plane.

An important source of information on relevant flow features can be obtained from the interpretation of surface flow visualization experiments. These show a geometric conicity, in that along rays emanating from a certain origin close to the wedge apex the

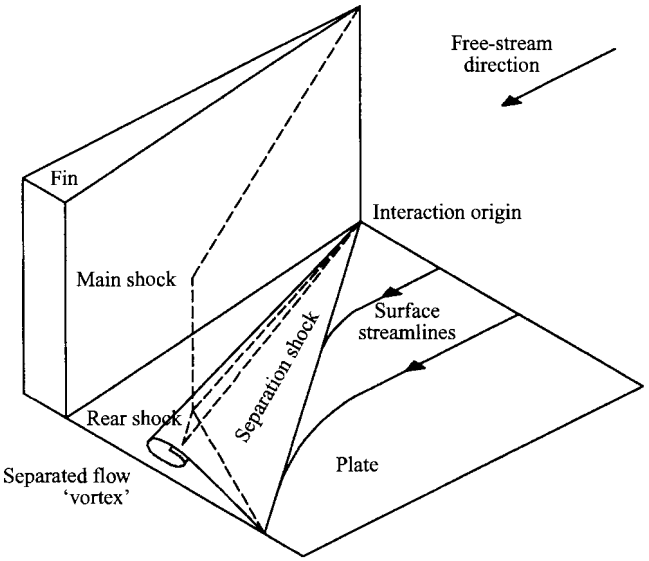

FIGURE 1. Conical interaction between a swept shock wave and a boundary layer.

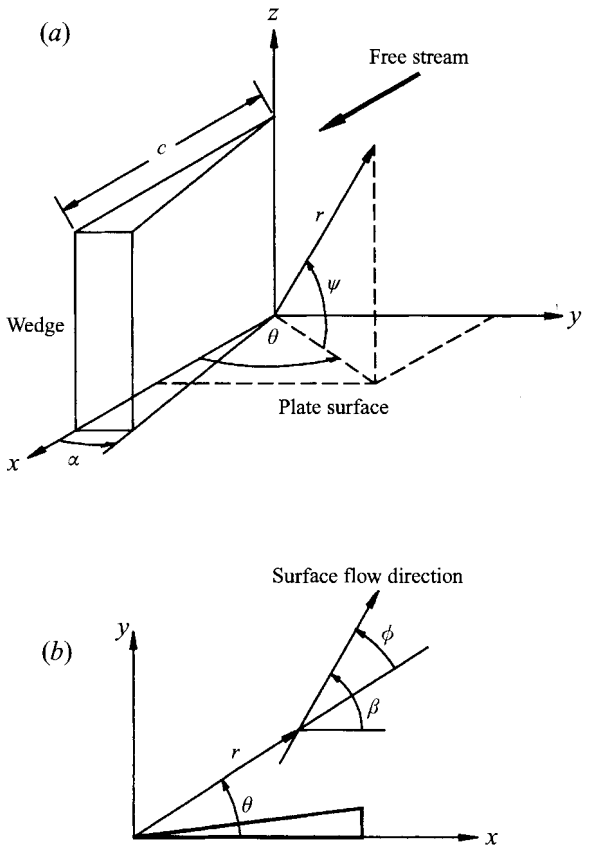

FIGURE 2. Definition of geometry and coordinate systems: (*a*) Cartesian and spherical/conical coordinate system; (*b*) surface flow description.

directions of the oil streaklines are to a large extent independent of the distance along the ray. The aim of the present investigation is to provide an analytical framework for the quantitative interpretation of such surface flow visualizations, in terms of corresponding cross-flow features, for conical interaction fields. To this end, the scaling structure of the interaction has to be considered first, in particular that of the viscous regions (Van Oudheusden 1995).

1.2. *Conical flow field description*

In a conical flow field all flow quantities are constant on rays through the conical centre of the flow field, which makes it beneficial to study such flows in a so-called cross-flow plane representation. Neglecting secondary effects, the conical centre of the fin–plate interaction lies at the intersection of the fin leading edge with the plate surface. The flow velocity vector is decomposed into a radial component U and cross-flow components V and W with regard to the conical reference frame (r, θ, ψ), see figure 2 and the Appendix for details. As in conical flow the flow pattern is invariant with r, its relevant features are revealed in the (θ, ψ) cross-flow plane. Also, the local flow direction ϕ at a point of the surface is a function only of the ray angle θ (see figure 2*b* for the definition of ϕ).

The topological structure of the cross-flow streamline pattern is characterized by its singular points, where the local velocity vector coincides with the ray direction and, hence, the cross-flow components V and W vanish. Singular points that lie on the surface correspond to lines in the surface flow patterns where the surface flow is directed along the conical ray, and where hence the local flow angle ϕ is zero. A relation between the surface pattern near a singular surface line and the topology of the corresponding cross-flow singularity will be established in §3.

For reference the surface flow direction representation and the cross-flow streamline pattern of the inviscid wedge flow are depicted in figure 3. In the (θ, ϕ)-plane the flow is represented by two straight line segments, $\phi = -\theta$ for $\theta > \sigma$ for the undisturbed flow upstream of the shock, and $\phi = \alpha - \theta$ for $\alpha < \theta < \sigma$ for the deflected flow behind the shock (α and σ denote the wedge angle and shock wave angle, respectively). The cross-flow streamlines are generated by the following expression:

$$\frac{\mathrm{d}\theta}{\mathrm{d}\psi} = \frac{V}{W} = \frac{v/u - \theta}{w/u - \psi} = \frac{\beta - \theta}{-\psi} \tag{1}$$

for small angles β, θ and ψ. Here u, v, w are the Cartesian velocity components and $\beta = \theta + \phi$ the local flow direction with respect to the undisturbed flow (figure 2*b*). The cross-flow pattern for a constant value of β corresponds to radially converging streamlines in the (θ, ψ)-plane. For the undisturbed flow at $\theta > \sigma$ the streamlines converge on $(0, 0)$, while for the deflected flow at $\alpha < \theta < \sigma$ they converge on $(\alpha, 0)$.

1.3. *Conical shock-wave/boundary-layer interactions*

To put the present study in perspective, a short summary is given here of the major flow features of the conical interaction as revealed by the existing body of experimental and numerical evidence, see again the reviews in Settles (1993) and Knight (1993). For weak shocks the flow in the boundary layer is deflected without displaying separation. As the streamlines in the boundary layer are deflected by a larger amount that those in the inviscid flow, a variation of the flow direction through the boundary layer is introduced, which gives rise to a streamwise vorticity component. McCabe (1966) considered the deflection of the surface streamlines using an inviscid vorticity transport

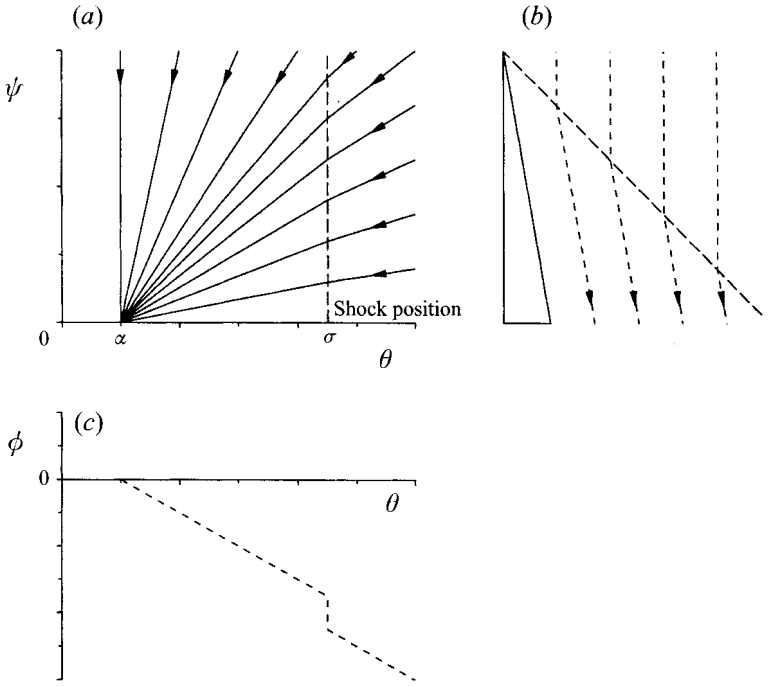

FIGURE 3. Conical representation of inviscid wedge flow (arbitrary units): (*a*) conical cross-flow streamline pattern; (*b*) surface projection of the inviscid streamline pattern; (*c*) conical surface flow direction.

approach. He derived an approximate expression for the surface flow deflection β_s as a function of the inviscid flow deflection β_e at the boundary layer edge, predicing that for small deflection angles $\beta_s \approx 3\beta_e$.

For sufficient shock strength the flow is forced to separate from the surface. According to Stanbrook (1960) incipient separation occurs when the surface flow deflection equals the shock angle, corresponding to a vanishing skin friction component normal to the interaction as in swept two-dimensional separation. Separation is reflected by a convergence of skin friction lines towards the separation line, while at reattachment a divergence of skin friction lines occurs. In a conical flow field the separation surface rolls up into a (conical) vortex. Topologically, the corresponding separated flow in the conical cross-flow plane consists of a separation-saddle/focus connection and a further attachment-saddle, in contrast to (swept) two-dimensional flow where a local separation has a closed saddle/centre/saddle structure. With a further increase of the shock strength the reversed flow under the vortex may induce a secondary separation (Korkegi 1976). Kubota & Stollery (1982) found evidence of the separated vortical flow region above the surface, and in addition a second vortex near the fin/plate intersection line, the latter being present even for weak interactions without boundary layer separation. This corner vortex was also reported in recent numerical studies (Knight 1993; Panaras 1992). The conical character of the interaction flow field has been further confirmed by extensive visualization experiments (Settles & Lu 1985; Alvi & Settles 1992), which reveal that the swept main shock bifurcates into an oblique separation shock and a nearly normal, but curved rear shock above the separated vortex flow (cf. figure 1).

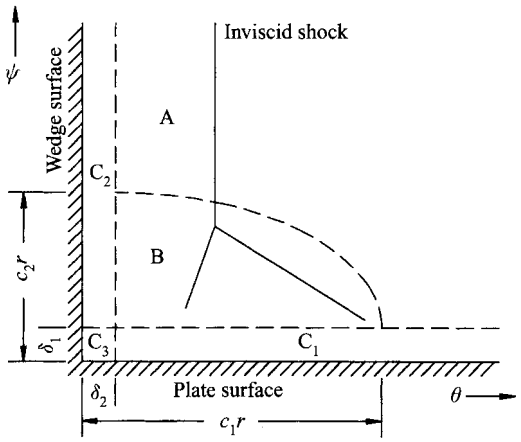

FIGURE 4. Schematic structure of the interaction region in the cross-flow plane. A: inviscid, irrotational flow; B: inviscid rotational flow; C: viscous flow.

1.4. *Three-layer flow models for viscous/inviscid interactions*

The structure of the interaction between a shock wave and a boundary layer, where the discontinuous pressure rise over the inviscid shock wave is incompatible with the normal boundary layer asumption of small streamwise gradients, can be described by a three-layer model. This 'triple deck' structure has commonly been used for the asymptotic analysis of both incompressible and compressible interactions in two-dimensional laminar flows (Stewartson 1974; Burggraf 1975). In the present study, this approach is applied to describe the flow structure of the conical interaction in the cross-flow plane (figure 4). It distinguishes an outer flow region (A), an inviscid interaction region (B), and viscous flow layers at the fin and plate surfaces (C), cf. Stollery (1975). The C-layers consist of viscous rotational flow, where 'viscous' is used here to imply that shearing stresses are significant and hence includes both laminar and turbulent stresses. Region A corresponds to the undisturbed flow, which is inviscid and (in the absence of shock curvature) irrotational. The intermediate region (B) consists of inviscid, rotational flow, where the pressure field of the inviscid flow is modified to accommodate the viscous layer, while simultaneously the displacing effect of the viscous layers is transferred to the outer flow. In this flow field structure it is possible to embed a local small-scale separation within the viscous layer, if an interacting boundary condition is used to represent the matching with the outer flow (Stewartson 1974; Burggraf *et al.* 1979; Veldman 1979). This *interacting* boundary layer differs from the classical boundary layer mainly in that its displacement effect on the inviscid flow is of leading order.

2. Quantitative and topological interpretation of surface flow patterns

2.1. *Interpretation of surface oil flow visualizations*

The streaklines in oil flow patterns are generally considered as being tangent to the direction of the skin friction on the surface. According to the molecular concept of viscosity, the viscous stress is parallel to the velocity shear which makes the skin friction direction equal to the limit of the flow direction when approaching the surface. Hence, the surface pattern is also referred to as 'surface streamlines' or 'limiting streamlines'. In general a separation line on the surface may be recognized as a line on which streaklines converge and where oil accumulates due to the shearing action of the

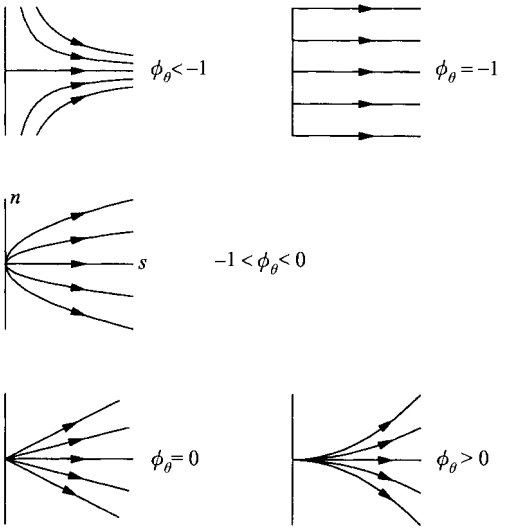

FIGURE 5. Geometry of surface streamlines.

flow. Conversely, attachment lines are accompanied by a divergent streakline pattern and an oil depletion effect. For a swept two-dimensional symmetry the surface pattern consists, in a first-order approximation, of streaklines either exponentially converging or diverging with respect to the singular line (Oskam, Vas & Bogdonoff 1976), corresponding to a separation and attachment line, respectively. Each is represented by a saddle singularity in the cross-flow plane normal to the singular line. For conical flow, on the other hand, it is possible for a nodal point to occur with either converging or diverging streaklines (Bulakh 1970; Bakker 1991). Here 'strong' convergence or divergence is required to obtain a saddle singularity in the cross-flow plane. In this context the term convergence is generally used to indicate that the streaklines asymptotically approach the singular line, whereas the situation where streaklines initially bend towards the singular line, but ultimately run parallel to it, is referred to as 'incomplete convergence' (Kubota & Stollery 1982). As the results of the present analysis will reveal, the transfer from incomplete to complete convergence in conical flow is not necessarily accompanied by the formation of a saddle point in the conical cross-flow plane.

2.2. *Topological considerations in conical flow*

As already mentioned the convergence and divergence lines correspond to singular points in the cross-flow plane. A direct relation between the streakline pattern and the nature of the corresponding singularity for the case of inviscid, isentropic conical flow was given by Bakker (1991), showing that three types of first-order surface singularities are possible: attachment and separation saddles, and a stable node (i.e. with inflowing streamlines). For reference a summary of this result is given in the following section. This approach is very appealing as it quantifies the relation between the topology of the cross-flow field and the surface pattern as represented in the (θ, ϕ)-plane, rather than just the qualitative observation that flow separation is accompanied by '(strong) convergence of the streaklines', and flow attachment by '(strong) divergence of the streaklines'. In §3 this analysis will be extended to establish a similar relation when viscous effects are included. Taking a linearization of the streakline field near the singular line, its structure is represented by the local value of ϕ_θ, i.e. the partial derivative of ϕ with respect to θ, see figure 5 (Bakker 1991):

$\phi_\theta < -1$: converging streaklines;
$\phi_\theta = -1$: parallel streaklines (with zero curvature);
$-1 < \phi_\theta < 0$: diverging streaklines with negative curvature;
$\phi_\theta = 0$: radially diverging streaklines (zero curvature);
$\phi_\theta > 0$: diverging streaklines with positive curvature.

2.3. *Topology of conical surface singularities in inviscid flow (Bakker 1991)*

Assuming for convenience only small flow angles, the conical surface flow direction ϕ in inviscid flow is given by $\phi = V/U$, hence, at a singular line we have $\phi = 0$ and $\phi_\theta = V_\theta/U$. The structure of the singularity is obtained from a local linearization of the cross-flow streamline pattern, which in general near the surface is (where W_θ vanishes identically)

$$\frac{\mathrm{d}\theta}{\mathrm{d}\psi} = \frac{V}{W} = \frac{V_\theta \theta + V_\psi \psi}{W_\psi \psi}. \tag{2}$$

Evaluation of the continuity and momentum equations at the surface singularity yields the additional conditions $V_\psi = 0$ and $V_\theta + W_\psi + 2U = 0$ (see the Appendix), with which the above expression can be replaced by the following equivalent linear system:

$$\begin{pmatrix} \dot{\theta} \\ \dot{\psi} \end{pmatrix} = \begin{pmatrix} \phi_\theta & 0 \\ 0 & -(2+\phi_\theta) \end{pmatrix} \begin{pmatrix} \theta \\ \psi \end{pmatrix}. \tag{3}$$

Unless $\phi_\theta = -2$ or 0, for which the above system becomes degenerate and higher-order singularities have to be considered, the structure of the singularity is described by the eigenvalues of the matrix (see e.g. Jordan & Smith 1977), as

$\phi_\theta < -2$: separation saddle;
$-2 < \phi_\theta < -1$: stable orthogonal node;
$\phi_\theta = -1$: stable star-like node;
$-1 < \phi_\theta < 0$: stable tangent node;
$\phi_\theta > 0$: attachment saddle.

Hence, the value of ϕ_θ establishes a direct relation between the structure of the surface flow pattern near a singular line and the topology of the related conical singularity. Note that the condition for a separation saddle to occur ($\phi_\theta < -2$) is more severe than that for streakline convergence ($\phi_\theta < -1$), as given in §2.2.

3. Conical surface singularities in viscous flow

3.1. *Scaling of the viscous layer*

The viscous layer is defined as the region of the flow adjacent to the surface where shear stresses have to be taken into account. As the viscous equations do not allow a strict conicity of the flow field in general, the major question to be addressed here is whether it is possible to devise a structure of the viscous layer that is compatible with the conical inviscid flow, and that produces a geometrically conical surface flow (skin friction pattern). The conical inviscid flow imposes conical boundary conditions on velocity components and thermodynamic properties (temperature, pressure and density). Note that the conicity of the surface flow pattern does not imply that the surface shear stress itself must be invariant with r. As long as both stress components display a similar scaling with r, the same shear direction results.

For the analysis of the viscous layer the standard thin shear layer approximations are adopted, namely that the pressure gradient normal to the wall is negligible, and that the velocity component normal to the wall is much smaller than the velocity

components parallel to the wall, which scale with the velocity of the inviscid flow. In accordance to the thin layer approximation only the shear stresses parallel to the surface are included.

To investigate whether the flow equations allow a viscous layer structure compatible with the conical inviscid flow, the assumption is made that the viscous layer shows similarity in the r-direction, in that it scales with a transversal lengthscale δ that is a function only of the projected ray length $r_p = r\cos\psi$ (for ψ small $r_p \approx r$, and the index p is omitted where no confusion arises). In a (r_p, θ, ζ) coordinate system, with $\zeta = z/\delta$, and for small ψ, we have

$$\frac{\partial}{\partial r} = \frac{\partial}{\partial r_p} + \frac{\zeta}{r}(1-\lambda)\frac{\partial}{\partial \zeta}, \quad \frac{\partial}{\partial \psi} = \frac{r}{\delta}\frac{\partial}{\partial \zeta}, \tag{4}$$

where λ relates to the viscous layer growth in the radial direction:

$$\lambda(r) = \frac{r}{\delta}\frac{\mathrm{d}\delta}{\mathrm{d}r}. \tag{5}$$

Consideration of the continuity equation reveals that the velocity component normal to the wall is one order in δ/r smaller than the other velocity components, and hence the following scaling is applied to obtain scaled velocity components (indicated by a prime) that are all of order one:

$$U/U^* = U'(r_p, \theta, \zeta), \quad V/U^* = V'(r_p, \theta, \zeta), \quad W/U^* = (\delta/r)\, W'(r_p, \theta, \zeta), \tag{6}$$

with U^* the velocity scale of the inviscid flow. Similarly, scales for the density and viscosity are denoted by ρ^* and μ^*. Under the assumption of similarity any r_p-dependence vanishes and the momentum equations for the r- and θ-directions become

$$\rho'[\zeta(1-\lambda)\, U'U'_\zeta + V'U'_\theta + W'U'_\zeta - V'^2] = \frac{r/\delta}{\rho^* U^{*2}}\tau_{1_\zeta}, \tag{7}$$

$$\rho'[\zeta(1-\lambda)\, U'V'_\zeta + V'V'_\theta + W'V'_\zeta + U'V'] = -\frac{p_\theta}{\rho^* U^{*2}} + \frac{r/\delta}{\rho^* U^{*2}}\tau_{2_\zeta}, \tag{8}$$

where τ_1 and τ_2 are the shear stress components in the r- and θ-directions, respectively. The ψ-momentum equation reduces to the well-known condition that in the thin shear layer estimate the transverse pressure gradient can be neglected as being of higher order:

$$p_\psi \sim \rho^* U^{*2}\delta/r. \tag{9}$$

If, furthermore, the energy equation is represented by a Crocco–Busemann relation (White 1991), similarity in the velocity directly implies similarity in the temperature as well. Alternatively, a transport energy equation can be used (Inger 1987), but as this allows a similar scaling as the momentum equations (under appropriate boundary conditions) the energy equation is not considered here any further. The conditions under which the viscous flow equations, (7) and (8), allow similarity (given conical boundary conditions) are

$$\lambda = \text{constant} \Rightarrow \delta \propto r^\lambda, \tag{10}$$

$$\tau_i r/\delta \sim \rho^* U^{*2} \Rightarrow \tau_i \sim \rho^* U^{*2}\frac{\delta}{r} \propto r^{\lambda-1} \quad (i = 1, 2). \tag{11}$$

The value of λ for which the above condition is satisfied depends on how the shear

stresses are related to the velocity field. For laminar flow the shear stress is directly related to the velocity gradient, as

$$\tau_i = \mu U_{i_z} = \frac{\mu}{\delta} U_{i_\zeta} \sim \frac{\mu^* U^*}{\delta}, \tag{12}$$

where U_1 stands for U and U_2 for V. Combination of (11) and (12) shows that the viscous layer scaling for laminar flow is given by

$$\delta \sim \left(\frac{\mu^* r}{\rho^* U^*}\right)^{1/2} = r\, Re_r^{-1/2} \Rightarrow \lambda = 1/2, \quad \tau_i \sim \rho^* U^{*2} Re_r^{-1/2}, \tag{13}$$

where Re_r is the Reynolds number based on r and the appropriate reference properties.

A dimensional estimate for large Reynolds number turbulent flow, where the turbulent shear stress dominates over the molecular stress in most of the viscous layer, is made using an eddy viscosity ϵ based on a mixing-length concept:

$$\tau_i = \rho\epsilon \frac{\partial U_i}{\partial z} = \rho \left(\frac{l}{\delta}\right)^2 \frac{\partial Q}{\partial \zeta} \frac{\partial U_i}{\partial \zeta} \sim \rho^* U^{*2}, \tag{14}$$

where l is the mixing length and Q a velocity scale which scales with U^*. In the standard mixing length approach Q would typically be the magnitude of the total velocity vector; it is, however, not further defined here. The above expression is not intended as an accurate description of the turbulent shear stress, but as the dimensional estimate of its dependence on r. In fact, l/δ and Q may contain arbitrary functions of ζ and θ, and even be different for τ_1 and τ_2, without violating the above estimate (which is therefore more widely applicable than the eddy viscosity concept itself). Combination of (11) and (14) yields the following scaling for a turbulent viscous layer:

$$\delta \sim r \Rightarrow \lambda = 1, \quad \tau_i \sim \rho^* U^{*2}. \tag{15}$$

This does not mean that δ and r are numerically of the same order of magnitude, but that the viscous layer thickness scales proportionally to r. Note that the shear stresses show no Reynolds number dependence, because of the omission of the effect of molecular viscosity, which applies to the limit of infinitely large Re. As an indication of the effect of the molecular shear stress at finite Reynolds numbers, let Blasius' approximate empirical expressions for turbulent boundary layer growth in two-dimensional incompressible zero-pressure-gradient flow be considered, which yields (Schlichting 1979)

$$\delta \sim r\, Re_r^{-1/5} \Rightarrow \lambda = 4/5, \quad \tau_i \sim \rho^* U^{*2} Re_r^{-1/5}, \tag{16}$$

whereas White (1991) suggests $\lambda = 6/7$ for improved agreement at higher Re_r. This indeed illustrates a very weak dependence of the shear stress on Re_r.

The above analysis shows that (for the turbulent part of the viscous layer), assuming a similarity in the velocity profiles, a similarity in the shear stress profiles also exists, provided there is similarity in the profiles of l/δ, which are statements consistent with each other. It is interesting to confront this result with the concept of equilibrium boundary layers, as derived by Clauser (1954, 1956) for two-dimensional incompressible flow. He showed that for certain free-stream conditions for which a conveniently defined pressure-gradient/wall-shear parameter is constant (including the case of zero pressure gradient), the velocity defect profiles display similarity when scaled with the shear stress velocity $u_\tau = (\tau_w/\rho)^{1/2}$. Using the momentum equation, he also showed that given this similarity no exact similarity of the shear stress profile can exist simultaneously. Tennekes & Lumley (1972), however, showed that this similarity

is possible in the sense of asymptotic invariance (Reynolds number similarity) for the case $c_f \ll 1$, which means for the part of the boundary layer where the relative velocity defect is small. Note that the present findings, which state similarity in both velocity and shear stress profiles do not correspond directly to Clauser's defect law where u_τ is the scaling velocity instead of the outer flow velocity. However, as under these assumptions u_τ is deduced to be invariant with the streamwise distance, there is no direct disagreement. Also, the model of Tennekes & Lumley predicts that for a very slow variation of u_τ an approximately linear growth of the boundary layer thickness δ results, which is also found here. We may therefore conclude that the present model is valid as the description for very large *Re*, but does not provide an exact *Re*-scaling similarity. In that sense it is only an approximately correct asymptotic model, giving a local approximation instead of being valid for the complete range of large *Re*. The reason for this is that *Re* influences essentially remain present, owing to the viscous origin of the wall shear stress even at very large *Re*, and which is introduced through the matching of the turbulent (defect) layer with the laminar sublayer at the wall.

3.2. *Asymptotic structure of the interaction flow*

Based on the above estimates the asymptotic scaling structure is discussed for the three-layer model of the interaction given in figure 4. The upper and middle layers (A and B) are essentially inviscid and show a conical similarity. The viscous layer (C_1), subjected to conical boundary conditions imposed by the inviscid flow, shows a conical extension in the direction along the surface, whereas normal to the surface the viscous layer thickness δ scales with r^λ ($\lambda = 1/2$ for laminar flow and $\lambda \approx 1$ for large-*Re* turbulent flow), with

$$\delta \sim r\, Re_r^{\lambda-1} \Rightarrow \tau_i \sim \rho^* U^{*2}\, Re_r^{\lambda-1}. \tag{17}$$

Note that this scaling only considers the dependence on r (the distance measured along a conical ray), and does not state that the viscous layer thickness should be necessarily invariant with θ. In the flow directly adjacent to the surface the molecular stresses are dominant even in turbulent flow, and the scaling thickness δ_{sub} of this 'laminar sublayer' is defined by

$$\tau_i \sim \mu^* U^*/\delta_{sub} \Rightarrow \delta_{sub} \sim r\, Re_r^{-\lambda}, \quad \delta_{sub}/\delta \sim Re_r^{1-2\lambda}. \tag{18}$$

Note that δ_{sub} is a scaling length and not the thickness of the laminar sublayer itself. The latter is formed from the total wall shear stress as $\delta_{lam} \sim \mu/(\rho u_\tau)$, which leads to the following estimates of the thickness and velocity scale of the laminar sublayer (see figure 6):

$$\delta_{lam} \sim r\, Re_r^{-(1+\lambda)/2}, \quad U^*_{lam} = U^*\, \delta_{lam}/\delta_{sub} \sim U^*\, Re_r^{-(1-\lambda)/2}. \tag{19}$$

It is interesting to observe that for a conical flow the similarity scaling obtained here with respect to the development of δ in the radial direction, is the same as that in the streamwise direction for a two-dimensional flow in a zero pressure gradient. Apparently the entrainment from the inviscid flow into the viscous layer can be considered to have a dimensionally similar effect, notwithstanding the conical growth in the spanwise direction.

For turbulent flow the wall shear stress is found to be nearly conical (independent of r), which corresponds to recently reported numerical results (Knight *et al.* 1992). For laminar flow the skin friction scales as $r^{-1/2}$. Note in comparison, that if a true conical similarity such as exists in the inviscid flow, were extended directly to the velocity field inside the viscous layer as well, the laminar skin friction would be predicted to scale with r^{-1}.

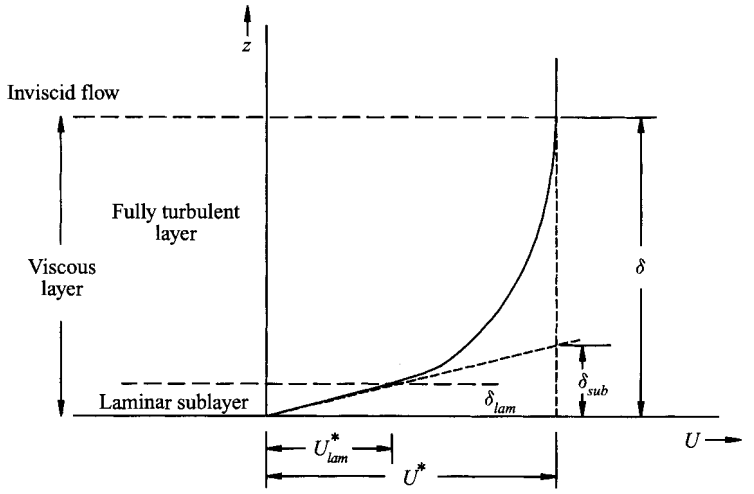

FIGURE 6. Definition of parameters in the scaling of the velocity profile in the turbulent viscous layer.

3.2.1. *Departure from conicity*

Departure from conicity of the interaction can result from non-conicity of the additional boundary conditions, such as a violation of the assumed conical pressure condition due to the interaction with the viscous layer (displacement effect). Evidently a conical viscous layer growth provides a conical boundary condition, yielding a conical inviscid region regardless of the magnitude of the interaction. Departure from conicity of the interaction due to the non-conical growth of δ (i.e. when $\lambda \neq 1$) can be considered, in the case of weak interaction, a second-order effect if $\delta \ll r$, which for $\lambda < 1$ is asymptotically satisfied for $r \to \infty$. For strong interaction, however, this is not the case and therefore strict conicity cannot be obtained. Hence, for turbulent flow the conditions for conicity are satisfied to a good approximation, whereas laminar interactions will possess a local conicity only.

Obviously the above (asymptotic) description fails near the conical origin, because the viscous layer thickness does not vanish with r going to zero, but instead has to match the undisturbed boundary layer thickness. This gives rise to the creation of the so-called inception zone, an area of non-conical flow near the wedge vertex before the approximate asymptotic pattern is established. Owing to the finite incoming boundary layer thickness, the virtual origin of the conical flow is located upstream of the wedge vertex (Settles 1993).

In addition to the viscous layer C_1 that results from the interaction of the shock and the existing boundary layer on the plate surface, a viscous layer also develops on the fin surface (region C_2). In the asymptotic state this layer develops under the influence of a conical inviscid flow, and therefore its dimensional scaling is similar to that of C_1 (though the numerical scaling factor may be different). As it develops from the fin leading edge it does not have to match an upstream condition. Still, it cannot display a conical development right from the leading edge, because of the non-conicity of the inviscid flow (B) in the inception region, caused by the non-conical interaction condition at the plate. Only when both C_1 and C_2 develop from the leading edge (as in double-wedge configuration) is a strict conicity possible right from the wedge vertex (Charwat & Redekeopp 1967).

3.3. *Topology of conical surface singularities in viscous flow*

In viscous flow all velocity components vanish at the wall and application of the limiting streamline concept yields for the conical flow direction angle $\phi = V_\psi/U_\psi = \tau_2/\tau_1$. A surface singularity is now obtained for $V_\psi = 0$, where then $\phi_\theta = V_{\theta\psi}/U_\psi$. Taking the wall compatibility conditions into account the linearized streamline pattern near the singularity is

$$\frac{\mathrm{d}\theta}{\mathrm{d}\psi} = \frac{V/\psi}{W/\psi} = \frac{V_{\theta\psi}\,\theta + \frac{1}{2}V_{\psi\psi}\,\psi}{\frac{1}{2}W_{\psi\psi}\,\psi}. \tag{20}$$

A further compatibility condition at the wall is obtained by taking the ψ-derivative of the continuity equation, which when evaluated at a conical singularity gives (see the Appendix)

$$V_{\theta\psi} + W_{\psi\psi} + 2U_\psi = -rU_{r\psi}, \tag{21}$$

assuming conical thermodynamic surface conditions (surface temperature and static pressure are independent of r, hence also $\rho_r = 0$ and $\mu_r = 0$). The scaling law of the shear stress in the radial direction, (17), reveals that $rU_{r\psi} = \lambda U_\psi$, while evaluation of (8) at the surface yields $p_\theta = \tau_{2_\psi}$, hence $V_{\psi\psi}/U_\psi = p_\theta/\tau_1$. Combining these results the linearized streamline pattern can be expressed by the following linear system, where all elements relate to properties of the flow near the surface:

$$\begin{pmatrix}\dot{\theta}\\ \dot{\psi}\end{pmatrix} = \begin{pmatrix}\phi_\theta & \frac{1}{2}p_\theta/\tau_1\\ 0 & -\frac{1}{2}(2+\lambda+\phi_\theta)\end{pmatrix}\begin{pmatrix}\theta\\ \psi\end{pmatrix}. \tag{22}$$

Excluding the degenerate cases $\phi_\theta = -(2+\lambda)$ or 0, the structure of the singularity is determined by the value of ϕ_θ as follows:

$\phi_\theta < -(2+\lambda)$: separation saddle;
$-(2+\lambda) < \phi_\theta < -(2+\lambda)/3$: stable tangent node;
$\phi_\theta = -(2+\lambda)/3$: stable node (star-like when $p_\theta = 0$, otherwise degenerate);
$-(2+\lambda)/3 < \phi_\theta < 0$: stable orthogonal node;
$\phi_\theta > 0$: attachment saddle;

while the separatrix angle γ follows from (20) and (22), see Jordan & Smith (1977), as

$$\tan\gamma = \frac{W_{\psi\psi} - 2V_{\theta\psi}}{V_{\psi\psi}} = -\frac{\tau_1}{p_\theta}(2+\lambda+3\phi_\theta). \tag{23}$$

3.4. *Structure of the singularity at the intersection line*

The conical singularity at the intersection line between the fin and plate (region C_3 in figure 4) needs separate attention, because the previous expressions for ϕ and ϕ_θ become degenerate, as both U_ψ and V_ψ vanish. The alternative expressions are found by letting both θ and ψ go to zero simultaneously, yielding $\phi = V_{\theta\psi}/U_{\theta\psi}$ and $\phi_\theta = V_{\theta\theta\psi}/U_{\theta\psi}$. Furthermore, taking first and second derivatives (with respect to θ and ψ) of the continuity equation (A 3), and evaluating the results at the intersection point yields $W_{\theta\psi} = W_{\theta\theta\psi} = V_{\theta\psi} = V_{\theta\theta\psi} = 0$. The linearized streamline pattern near the intersection singularity then follows from

$$\frac{\mathrm{d}\theta}{\mathrm{d}\psi} = \frac{V/(\theta\psi)}{W/(\theta\psi)} = \frac{V_{\theta\theta\psi}\,\theta}{W_{\theta\psi\psi}\,\psi}. \tag{24}$$

By taking the $\theta\psi$-derivative of the continuity equation and assuming that for both viscous layer scalings the same value of λ applies, the following condition is obtained:

$$V_{\theta\theta\psi} + W_{\theta\psi\psi} + (2+2\lambda)\,U_{\theta\psi} = 0. \tag{25}$$

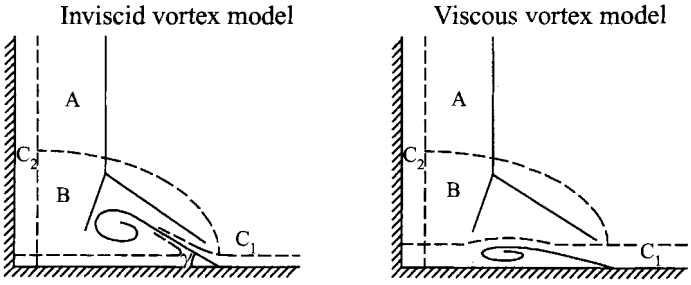

FIGURE 7. Fitting of a separation vortex structure in the asymptotic scaling model.

Hence, upon division by $U_{\theta\psi}$, (24) describing the linearized singularity is written as

$$\begin{pmatrix} \dot{\theta} \\ \dot{\psi} \end{pmatrix} = \begin{pmatrix} \phi_\theta & 0 \\ 0 & -(2+2\lambda+\phi_\theta) \end{pmatrix} \begin{pmatrix} \theta \\ \psi \end{pmatrix}. \tag{26}$$

Again excluding the degenerate cases, the structure of the intersection singularity is determined as follows:

$\phi_\theta < -(2+2\lambda)$:	separation saddle;
$-(2+2\lambda) < \phi_\theta < -(1+\lambda)$:	stable orthogonal node;
$\phi_\theta = -(1+\lambda)$:	stable star-like node;
$-(1+\lambda) < \theta_\theta < 0$:	stable tangent node;
$\phi_\theta > 0$:	attachment saddle.

3.5. *Separation/reattachment structures in the asymptotic interaction model*

Based on the above results of the topological description, the issue of how to fit the singularity structure, in particular that of the separation, into the asymptotic scaling approach of figure 4 is now considered. Concerning the assumed separation structure, with a conjectured vortical structure in the flow field, some controversy may exist as to whether it should be a feature of the inviscid interaction region **B**, or of the viscous layer C_1 (as is illustrated in figure 7). In the former case the vortex structure would grow essentially in a conical way with the height of the region scaling with r (similar to the spanwise growth but probably to a lesser extent), whereas the 'viscous vortex' concept would involve a vertical scaling with δ.

The 'inviscid vortex' concept would be comparable to the leading edge separation on delta wings, where the development of secondary separation may also be observed. In that case the primary flow separation of the interaction should be regarded as a process in which the shear layer detaches from the surface and rolls up into the vortex core, the detached shear layer and vortex core (both viscous regions) being separated from the viscous surface layer by a region of essentially inviscid flow. This concept would lead to the view that, though initially the vortex is necessarily embedded inside the viscous layer, with downstream development it eventually rises above this layer and establishes itself in the inviscid flow interaction region. The secondary separation, which as revealed in experimental observation develops some distance downstream of the vertex, can then be considered as the effect of the inviscid vortex on the surface shear layer under it. In this concept the interacting boundary layer model proposed in §1.4 for the description of the interaction is no longer valid, and a more complex asymptotic interaction structure would be needed to model the details of the separation region, the separated shear layer and vortex core. If this were true, the topological

description presented here becomes questionable, as it uses a viscous layer scaling derived from applying the three-layer approach directly to the entire viscous surface layer.

The 'viscous vortex' concept on the other hand describes the flow separation as a local structure inside the viscous shear layer, which can be embedded in the three-layer model. The flow separation in this case does not involve a separation of the complete viscous shear layer, but is reflected in large cross-flow gradients in the direction normal to the surface and a significant local thickening of the viscous region, which can be considered as essentially an interacting boundary layer.

A strong argument in favour of the viscous vortex model is that the separation of the boundary layer flow, caused by the shock-induced pressure gradient, is clearly a viscous vortex in (swept-)two-dimensional flows. On the other hand, the apparent conicity of the structure, as indicated by experimental and numerical studies, may seem to support the inviscid vortex concept. Here, any initial non-conicity may be partially attributable to the effect of the inception region, assuming that the true asymptotic structure is established only sufficiently far downstream. Note, however, that for turbulent flows the observation of (asymptotic) conicity of the flow field is not in conflict with the viscous vortex concept, as in that case δ develops nearly proportional to r ($\lambda \approx 1$).

In the case of separation or attachment the scaling of the separatrix angle γ is derived from (23) to be

$$\tan\gamma = \frac{W_{\psi\psi} - 2V_{\theta\psi}}{V_{\psi\psi}} \sim \frac{U^* r/\delta}{U^*(r/\delta)^2} = \frac{\delta}{r}. \tag{27}$$

This estimate is compatible with the viscous vortex concept, whereas for an inviscid vortex approach we would have expected $\tan\gamma \sim 1$, and consequently $p_\theta \sim \rho^* U^{*2}\delta/r$. From evaluation of the Navier–Stokes equations near a conical saddle singularity at the wall, the pressure gradient normal to the wall is found to be $p_z = \mu w_{zz}$. Transferring this to the conical coordinate frame the following relation is obtained:

$$p_\psi = \frac{\mu}{r}(W_{\psi\psi} + 2U_\psi) = \frac{p_\theta \tan\gamma + 2(1-\lambda)\tau_1}{3} \sim p_\theta \tan\gamma \tag{28}$$

from which, with $\tan\gamma \sim \delta/r$ and $p_\theta \sim \rho^* U^{*2}$, follows that at most $p_\psi \sim \rho^* U^{*2}\delta/r$. As this is of the same order as the term normally neglected in the thin shear layer approximation, see (9), this confirms that the shallow separation (with $\gamma \sim \delta/r$) occurring in the viscous vortex model does not violate the thin layer approximations used in the scaling model.

4. Application in the analysis of experimental flow visualizations

4.1. *Experimental arrangement*

Visualization experiments have been carried out in a 15 cm supersonic blow-down wind tunnel at a Mach number of the undisturbed flow of 2.94 (Van Oudheusden, Nebbeling & Bannink 1994). Three wedge-shaped fins, with a chord of 140 mm, height of 120 mm and an apex angle of 5°, 9° or 13°, were used to generate shock waves to interact with the boundary layer on the test section sidewall. The thickness of the undisturbed boundary layer at the location of the wedge leading edge is about 6 mm ($Re_\delta \approx 2.5 \times 10^5$). Results of the flow visualizations for the weakest and the strongest interaction are shown in figure 8.

(*a*)

(*b*)

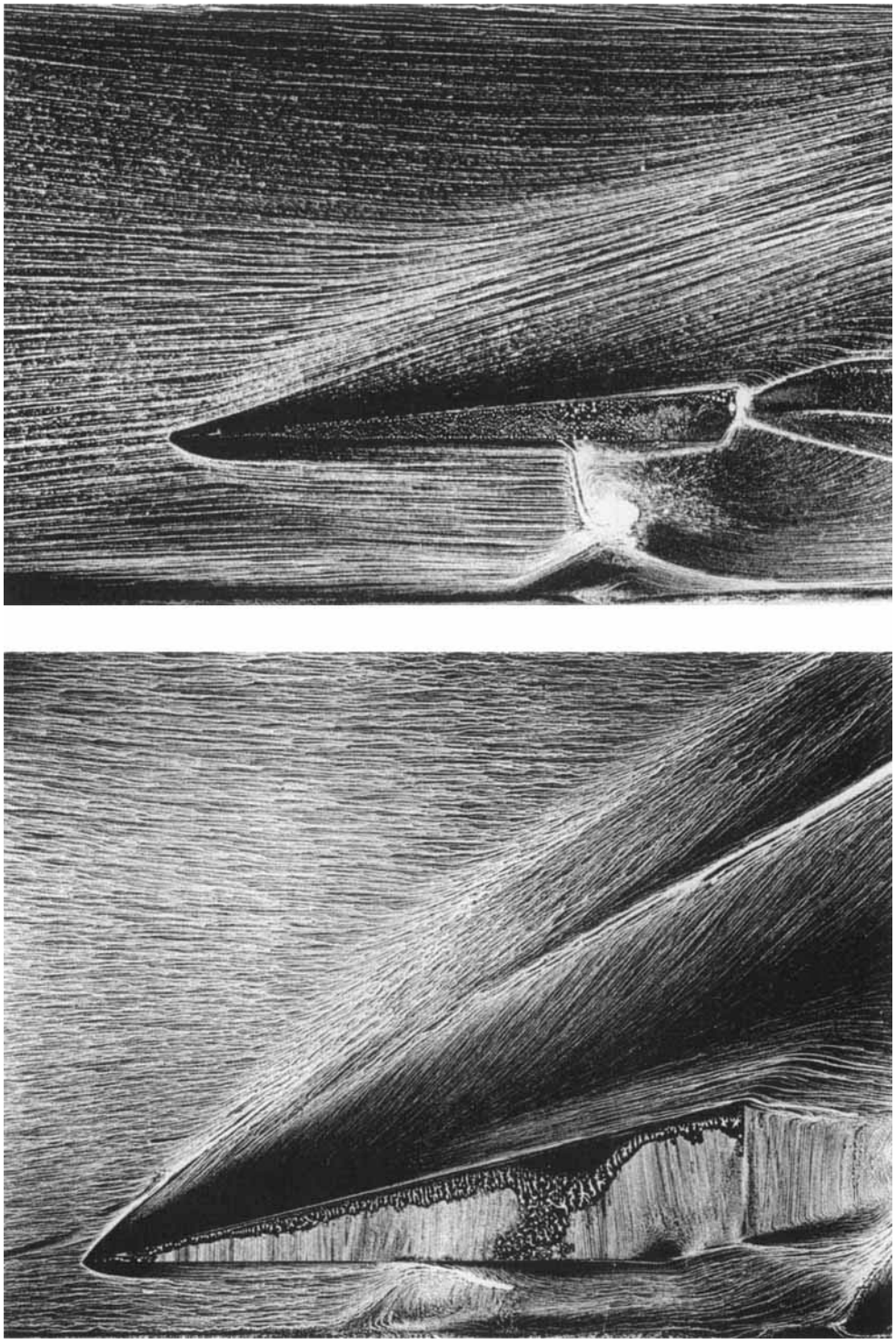

FIGURE 8. Oil flow visualization of the interaction for wedge angle (*a*) 5°, and (*b*) 13°.

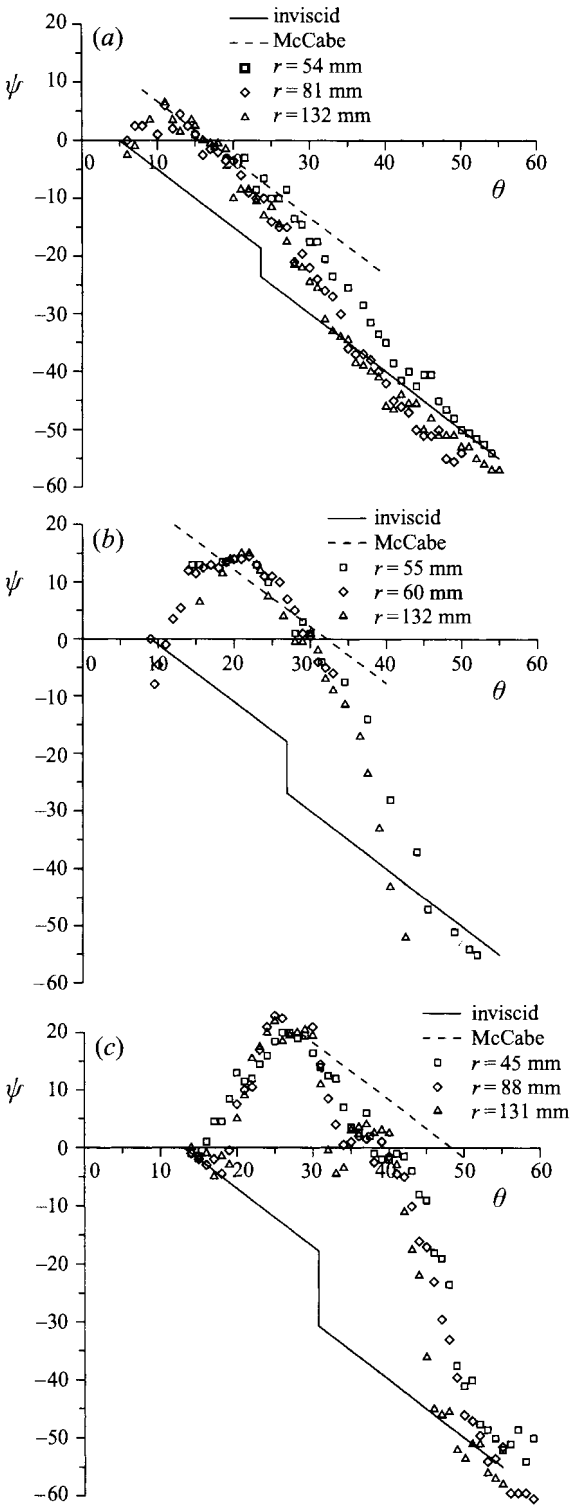

FIGURE 9. Conical surface flow direction: (*a*) $\alpha = 5°$, (*b*) $\alpha = 9°$, (*c*) $\alpha = 13°$.

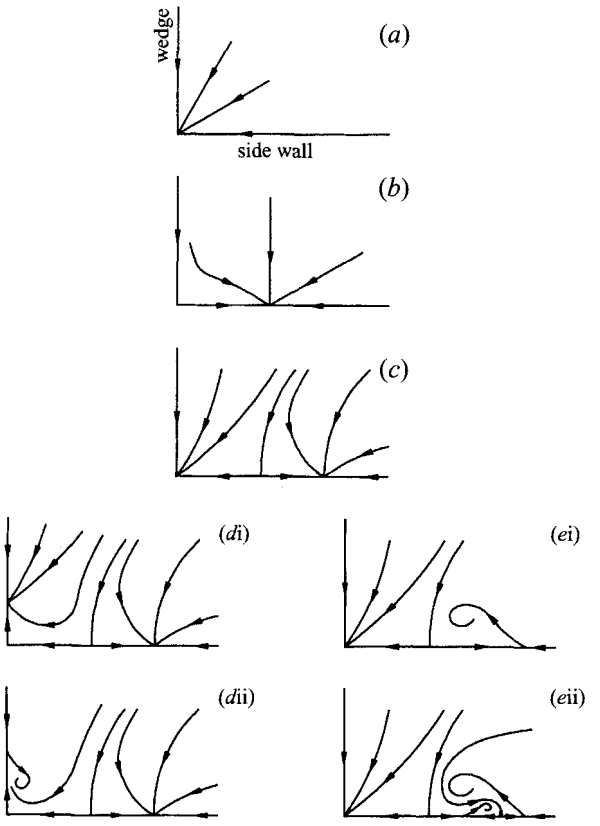

FIGURE 10. Evolution of the conical cross-flow pattern and bifurcation of the singularities.

The oil flow picture for the 5° wedge shows a deflection of the flow without the strong convergence and oil accumulation effect normally indicating flow separation. The result for the 13° wedge on the other hand, displays a complex flow structure of approximately conical structure. Note that some three-dimensionality is present in the undisturbed boundary layer, due to transverse pressure gradients which the boundary layer has experienced in the nozzle section of the wind tunnel. Conical surface flow directions measured at different circular trajectories from the wedge apex, are given in figure 9. The inviscid flow direction and the surface flow deflection according to McCabe's theory have been indicated in the graphs as well.

4.2. *Bifurcations of the cross-flow singularity pattern*

Topological changes in the cross-flow pattern may occur under the effect of gradual changes in the governing flow conditions (shock strength, Mach or Reynolds number) or in its downstream development. These changes are reflected by bifurcations of the singularities in the cross-flow plane. The following section provides a discussion of the conjectured flow field topology of the interaction in the cross-flow plane for increasing shock strengths, which is subsequently used as a general framework for the interpretation of the experimentally obtained flow visualization results. The structure of the flow pattern and its further bifurcations are discussed with regard to the schematic cross-flow plane representations in figure 10. The bifurcations that are discussed are those that are both topologically possible and physically likely in the light of existing experimental evidence (Settles 1993). Only a topological order is considered,

in that subsequent structures are assumed to have evolved from a previous simpler structure by means of an additional bifurcation. For independent bifurcations of different singularities there is no topological preference concerning the order in which they occur. The order in which bifurcations occur in reality is only revealed from physical evidence.

A first identification of the structure of the basic flow field is obtained from the cross-flow pattern for the inviscid flow (figure 3), which contains a single (star-like) node at the intersection of the wedge and plate surfaces. The introduction of viscosity into the flow description essentially changes the governing physics and cannot be considered as a continuous perturbation. However, the viscous flow for a zero wedge angle is topologically equivalent to that of the inviscid flow, with a single (not necessarily star-like) node at the plate–fin junction.

The first bifurcation of the junction node results in a node on the plate wall and a saddle at the junction (figure 10*b*). The node is associated with the deflecting effect of the shock wave, and corresponds to a singular ray dividing the streakline pattern into two regions. The outboard regions consists of the streaklines originating from upstream of the fin leading edge and deflected by the pressure rise over the shock wave, while in the inboard region streaklines originate from the fin–plate intersection. The latter are driven by the part of the flow that is initially directed towards the fin surface and subsequently deflected outwards through the attachment-saddle flow near the intersection corner.

Figure 10(*c*) shows the result of a further bifurcation, where the junction saddle has evolved into a node and with an additional attachment saddle, located between the junction and the outboard node near the shock wave. For increasing shock strength the latter node is observed to evolve into a separation saddle, which is assumed to be associated with a 'vortical' focus in the flow field above the wall (figure 10*e*i), while figure 10(*e*ii) shows the development of a secondary separation. The attachment streamline separates the flow that is directly deflected by the shock wave and which rolls up into the vortex core from the part of the flow that is directed along the fin, which is identified by the node at the fin. The possible further bifurcation of this junction node is shown in figure 10(*d*), first into a separation saddle and node at the fin (figure 10*d*i). This may develop further into a corner vortex as reported by Kubota & Stollery (1982), by forming a separation saddle on the fin and in figure 10(*d*ii). However, it is not possible to discriminate between the situations of figures 10(*d*i) and 10(*d*ii) on the basis of flow visualization on the plate surface alone. Supporting evidence of a corner vortex can therefore only be obtained if flow visualization is applied to the fin surface as well.

4.3. *Interpretation of the experimental flow field visualizations*

The experimentally obtained surface flow visualizations are now discussed in terms of the cross-flow topologies in figure 10. Note that although the analysis of § 3 can provide a quantitative estimation of the singularities that occur on the surface itself, it gives no direct information about the structure of (possible) singularities inside the flow field and in that respect a certain amount of conjecture is therefore present in the proposed flow field structures.

4.3.1. *Wedge angle* 5°

The situation for the wedge angle $\alpha = 5°$ appears to be in good accordance with the non-separated deflection theory of McCabe (1966). A conical singularity appears for $\theta = 17°$, which is well inboard of the shock wave, and with a local value of ϕ_θ of

approximately -1, denoting a parallel streakline pattern and incomplete convergence. At the intersection of fin and plate surfaces ϕ_θ is positive, which corresponds to an attachment saddle point. Outboard of the incomplete convergence line the streakline direction becomes gradually that of the undisturbed flow. A slight departure from conicity is observed in that the extent of the upstream influence region decreases with increasing distance from the wedge vertex, and the undisturbed flow direction is approached at smaller values of θ. This can be interpreted as an initially stronger spanwise growth, which corresponds to the inception region and the displacement of the virtual conical origin to a position upstream of the wedge vortex. Overall, there appears to be no significant topological change with streamwise distance of the cross-flow pattern, which possesses the structure of figure 10(*b*).

4.3.2. *Wedge angle* 9°

Apart from the direct vicinity of the junction line, the results for a wedge angle $\alpha = 9°$ are qualitatively similar to those of the previous case. However, the plate singularity occurring near $\theta = 30°$ lies slightly beyond the inviscid shock position, which is Stanbrook's condition for incipient separation (Stanbrook 1960). Also, the value of the slope of ϕ near the singularity significantly differs from -1, and has increased to approximately $\phi_\theta = -2.8$ which means complete convergence of the streaklines. Though it clearly differs from the parallel streakline pattern for the weak deflection case, the McCabe prediction seems to give a reasonable average streakline direction for a large region inboard of the convergence line. The above value of ϕ_θ is approximately that for which the singularity changes from a node to a saddle point, and together with the observation that the deviation from the unseparated theory is not very large, the present situation can be described as that of incipient separation.

The streakline direction data near the junction line indicate a large negative value of ϕ_θ at the junction itself, and a further singularity with a large positive slope a few degrees outboard the wedge. If these data are reliable, they indicate the existence of a separation saddle at the junction and an attachment saddle slightly outboard the junction. This corresponds to the structure in figure 10(*d*) (where the nature of the singularity on the fin surface can only be determined from the streakline pattern on the wedge, which is not available). As mentioned, the structure of the outboard singularity near the shock wave may be in transition from the nodal structure of figure 10(*d*) to that of a separation saddle as in figure 10(*ei*). Also, in this case there appears to be no significant downstream development of the flow topology.

4.3.3. *Wedge angle* 13°

In the flow pattern for the wedge angle $\alpha = 13°$ two distinct areas can be discerned with regard to the structure of the streakline pattern near the shock position. For distances from the wedge vertex up to approximately 80 mm only one singularity is present, whereas for larger distances two additional singularities appear. In the first region the singularity occurs at about $\theta = 38°$, which is well outboard of the inviscid shock wave. Also, the local gradient ϕ_θ is quite steep, indicating a separation saddle structure in the cross-flow plane. The singularity at the junction appears to be either a single attachment saddle (positive ϕ_θ), or a node with an attachment saddle located close to the junction, comparable to figure 10(*ei*). In the second region further downstream a second separation structure develops in the region between 32° and 35°. At first the flow between this second structure and the outboard singularity shows a shallow plateau at a small value of ϕ, indicating a nearly radial pattern of streaklines. Further downstream the curvature of the streaklines in this region increases. Although

in the first region the singularities of the secondary separation structure are absent, some indication of its development is given by irregularities in the $\phi(\theta)$-curve in the region near $\theta = 35°$.

Near the junction substantial evidence is given of a nodal singularity ($\phi_\theta \approx -1$), with an attachment saddle at $\theta = 18°$ to $20°$. The variation in streakline direction between this attachment and the secondary separation saddle is quite large (ϕ in the order of $20°$), which results in a strongly curved streakline pattern. The singularity pattern is comparable to that of figure 10(*e*ii).

Surprisingly, although the result for $\alpha = 9°$ seemed to indicate at least the possibility of a corner vortex separating from the fin surface of the type of figure 10(*d*ii), the results for $\alpha = 13°$ provide no evidence for this. Such a separation structure would at least require a saddle structure of the junction singularity, but instead a nodal structure is found. As the present experiments did not include visualization of the surface flow on the fin, no evidence is available either supporting or contradicting such a structure. A description of the flow structure directly near the fin is therefore not further attempted here.

5. Conclusions

An investigation was made of the conical scaling of the flow equations in order to describe the asymptotic structure of the swept interaction of a shock-wave and a boundary layer. A three-layer flow model of the interaction was applied, assuming an approximate conicity of the inviscid region of the flow, while the viscous layers of the interaction flow directly adjacent to the solid surfaces are considered as interacting boundary layers. The analysis reveals that by applying a transverse scaling of the viscous regions, an approximate similarity structure is obtained which is compatible with the conditions imposed by the conical inviscid flow. In the case of turbulent flow the viscous layer growth is approximately conical, with the shear stress being invariant with the radial distance. For laminar flow, with $\delta \propto r^{1/2}$ the inviscid flow remains weakly *Re*-dependent through the interaction condition, which results in the flow field becoming conical probably only in a local sense. Departure from conicity is evident in the inception region due to the matching with the incoming boundary layer.

The result of this analysis assists in a quantitative interpretation of surface flow visualizations, in terms of the topology of the corresponding cross-flow streamline pattern. Incorporating the results of the viscous layer scaling establishes, together with the viscous no-slip condition and the continuity equation, a description of the linearized cross-flow field near the singularity. It was shown that for separation/attachment which is compatible with the assumed conicity of the inviscid pressure field, the separatrix angle is of order δ/r and the normal pressure gradient is of the same order as in the thin shear layer approximation. This means that such a separation/attachment does not violate the underlying assumptions of the analysis, and can be incorporated within the viscous region of the flow field model (interacting boundary layer instead of shear layer detachment).

As an illustration, the method was applied to the analysis of surface oil flow visualizations of the swept interaction of a shock wave with a turbulent boundary layer at a free-stream Mach number of 2.94.

The work was supported by the European Space Research and Technology Centre ESTEC. The authors furthermore gratefully acknowlege the valuable comments provided by Professor P. G. Bakker.

Appendix. Coordinate system and wall compatibility relations in the conical flow field description

A.1. *Coordinate systems for a conical description of the flow field*

A Cartesian coordinate system (x, y, z) is defined with x in the direction of the undisturbed flow, y along the plate surface and z normal to the plate (figure 2), and with corresponding velocity components denoted by (u, v, w). A conical coordinate system (r, θ, ψ) is introduced through a spherical projection, with r the radius, θ the meridian angle and ψ the azimuthal angle:

$$x = r\cos\theta\cos\psi, \quad y = r\sin\theta\cos\psi, \quad z = r\sin\psi. \tag{A 1}$$

The conical velocity components (U, V, W) are defined with respect to a locally aligned orthonormal vectorial base: $\boldsymbol{e}_r = \operatorname{grad} r$, $\boldsymbol{e}_\theta = r\operatorname{grad}\theta$, $\boldsymbol{e}_\psi = r\operatorname{grad}\psi$, and are related to the Cartesian velocity components (u, v, w) as

$$\left.\begin{aligned} U &= u\cos\theta\cos\psi + v\sin\theta\cos\psi + w\sin\psi, \\ V &= -u\sin\theta + v\cos\theta, \\ W &= -u\cos\theta\sin\psi - v\sin\theta\sin\psi + w\cos\psi. \end{aligned}\right\} \tag{A 2}$$

The continuity equation expressed in these conical coordinates is given by

$$\frac{1}{r}(r^2\cos\psi\rho U)_r + (\rho V)_\theta + (\cos\psi\rho W)_\psi = 0, \tag{A 3}$$

where an index indicates the derivative with respect to the respective coordinate.

A.2. *Compatibility conditions at conical singular points on the surface*

In the following a number of wall compatibility conditions are derived for conical singularities on the surface, without assuming conicity of the flow field itself however.

A.2.1. *Inviscid flow*

The inviscid flow equations for conservation of momentum in the three coordinate directions are

$$rUU_r + \frac{1}{\cos\psi}VU_\infty + WU_\psi - V^2 - W^2 = -\frac{r}{\rho}p_r, \tag{A 4}$$

$$rUV_r + \frac{1}{\cos\psi}VV_\theta + WV_\psi + UV - \tan\psi VW = -\frac{1}{\rho\cos\psi}p_\theta, \tag{A 5}$$

$$rUW_r + \frac{1}{\cos\psi}VW_\theta + WW_\psi + \tan\psi V^2 + UW = -\frac{1}{\rho}p_\psi. \tag{A 6}$$

For inviscid flow the velocity condition at the impermeable surface at $\psi = 0$ is

$$W(r, \theta, 0) = 0 \Rightarrow W_r = W_\theta = 0. \tag{A 7}$$

Evaluation of the continuity equation (A 3) at a conical surface singularity (where $V = 0$) yields

$$\rho(V_\theta + W_\psi + 2U) = -r(\rho U)_r, \tag{A 8}$$

while eliminating the pressure from (A 5) and (A 6) gives

$$V_\psi(V_\theta + W_\psi + U) = -r\frac{UV_r\rho_\psi}{\rho} - r(UV_r)_\psi + r(UW_r)_\theta. \tag{A 9}$$

In the case of a conical flow field the right-hand sides of (A 8) and (A 9) vanish, yielding the following two conditions which apply to a surface singularity:

$$V_\psi = 0 \quad \text{and} \quad V_\theta + W_\psi + 2U = 0. \tag{A 10}$$

A.2.2. *Viscous flow*

In viscous flow all velocity components vanish at a solid surface, hence

$$\left.\begin{aligned} U(r,\theta,0) = 0 &\Rightarrow U_r = U_\theta = 0, \\ V(r,\theta,0) = 0 &\Rightarrow V_r = V_\theta = 0, \\ W(r,\theta,0) = 0 &\Rightarrow W_r = W_\theta = 0. \end{aligned}\right\} \tag{A 11}$$

Evaluating the continuity equation (A 3) at the wall leads to the additional condition that

$$W_\psi(r,\theta,0) = 0 \Rightarrow W_{r\psi} = W_{\theta\psi} = 0. \tag{A 12}$$

For viscous flow a conical singular point on the surface occurs when $V_\psi = 0$. By taking the ψ-derivative of (A 3), a further compatibility condition at the wall is obtained, which when evaluated at the singularity yields

$$V_{\theta\psi} + W_{\psi\psi} + 2U_\psi = -\frac{r(\rho U_\psi)_r}{\rho}. \tag{A 13}$$

When the thermodynamic surface conditions are conical, i.e. both the surface temperature and static pressure are independent of r, then $\rho_r = 0$ also, and as a result the above condition reduces to

$$V_{\theta\psi} + W_{\psi\psi} + 2U_\psi = -rU_{r\psi}. \tag{A 14}$$

Note that in the above discussion only the thermodynamic surface conditions were assumed to be conical, but not the velocity field itself.

REFERENCES

ALVI, F. S. & SETTLES, G. S. 1992 Physical model of the swept shock wave/boundary-layer interaction flowfield. *AIAA J.* **30**, 2252–2258.

BAKKER, P. G. 1991 *Bifurcations in Flow Patterns*. Kluwer.

BULAKH, B. M. 1970 *Nonlinear Conical Flow*. Translated from the Russian, Delft University Press (1985).

BURGGRAF, O. R. 1975 Asymptotic theory of separation and reattachment of a laminar boundary layer on a compression ramp. *AGARD CP-168, Flow Separation*, Paper 10.

BURGGRAF, O. R., RIZZETA, D., WERLE, M. J. & VASTA, V. N. 1979 Effect of Reynolds number on laminar separation of supersonic stream. *AIAA J.* **17**, 336–343.

CHARWAT, A. F. & REDEKEOPP, L. G. 1967 Supersonic interference flow along the corner of intersecting wedges. *AIAA J.* **5**, 480–488.

CLAUSER, F. H. 1954 Turbulent boundary layers in adverse pressure gradients. *J. Aero. Sci.* **21**, 91–108.

CLAUSER, F. H. 1956 The turbulent boundary layer. *Adv. Appl. Mech.* **4**, 1–51.

INGER, G. 1987 Spanwise propagation of upstream influence in conical swept shock/boundary layer interactions. *AIAA J.* **25**, 287–293.

JORDAN, D. W. & SMITH, P. 1977 *Nonlinear Ordinary Differential Equations*. Clarendon Press.

KNIGHT, D. D. 1993 Numerical simulation of 3D shock wave turbulent boundary layer interactions. *AGARD Rep. 792, Shock-Wave/Boundary-Layer Interactions in Supersonic and Hypersonic Flows*, pp. 3.1–3.32.

KNIGHT, D. D., BADEKAS, D., HORSTMAN, C. C. & SETTLES, G. S. 1992 Quasiconical flowfield structure of the three-dimensional single fin interaction. *AIAA J.* **30**, 2809–2816.

KORKEGI, R. H. 1976 On the structure of three-dimensional shock-induced separated flow regions. *AIAA J.* **14**, 597–600.

KUBOTA, H. & STOLLERY, J. L. 1982 An experimental study of the interaction between a glancing shock wave and a turbulent boundary layer. *J. Fluid Mech.* **116**, 431–458.

MCCABE, A. 1966 The three-dimensional interaction of a shock wave with a turbulent boundary layer. *Aero. Q.* **17**, 231–252.

OSKAM, B., VAS, I. E., & BOGDONOFF, S. M. 1976 Mach 3 oblique shock wave/turbulent boundary layer interactions in three dimensions. *AIAA Paper* 76-366.

PANARAS, A. G. 1992 Numerical investigation of the high-speed conical flow past a sharp fin. *J. Fluid Mech.* **236**, 607–633.

SCHLICHTING, H. 1979 *Boundary Layer Theory*, 7th edn. McGraw-Hill.

SETTLES, G. S. 1993 Swept shock/boundary-layer interaction – scaling laws, flowfield structure and experimental methods. *AGARD Rep. 792, Shock-Wave/Boundary-Layer Interactions in Supersonic and Hypersonic Flows*, pp. 1.1–1.40.

SETTLES, G. S. & LU, F. K. 1985 Conical similarity of shock/boundary-layer interactions generated by swept and unswept fins. *AIAA J.* **23**, 1021–1027.

STANBROOK, A. 1960 An experimental study of the glancing interaction between a shock wave and a turbulent boundary layer. *ARC CP 555.*

STEWARTSON, K. 1974 Multi-structured boundary layers on flat plates and related bodies. *Adv. Appl. Mech.* **14**, 145–239.

STOLLERY, J. L. 1975 Laminar and turbulent boundary-layer separation at supersonic and hypersonic speeds. *AGARD CP-168, Flow Separation*, Paper 20.

TENNEKES, H. & LUMLEY, J. L. 1972 *A First Course in Turbulence*. MIT Press.

VAN OUDHEUSDEN, B. W. 1995 The viscous layer scaling in conical flow interactions. *2nd ASME/JSME Symp. on Transitional and Turbulent Compressible Flows, Hilton Head, USA, 13–18 August 1995, FED*-Vol. 224, pp. 109–116.

VAN OUDHEUSDEN, B. W., NEBBELING, C. & BANNINK, W. J. 1994 Surface flow visualization of a glancing shock-wave boundary-layer interaction. *Rep.* LR-771. Delft University of Technology, Dept. Aerospace Engineering.

VELDMAN, A. E. P. 1979 A numerical method for the calculation of laminar, incompressible boundary layers with strong viscous-inviscid interaction, *NLR Rep.* TR 79023U.

WHITE, F. M. 1991 *Viscous Fluid Flow*, 2nd edn. McGraw-Hill.